

Pedro Baptista de Castro^{A,B*}, Kensei Terashima^{A*}, Takafumi D. Yamamoto^A, Suguru Iwasaki^C, Ryo Matsumoto^A, Shintaro Adachi^A, Yoshito Saito^{A,B}, Hiroyuki Takeya^A and Yoshihiko Takano^{A,B}
^ANational Institute for Materials Science, 1-2-1 Sengen, Tsukuba, Ibaraki 305-0047, Japan

^BUniversity of Tsukuba, 1-1-1 Tennodai, Tsukuba, Ibaraki 305-8577, Japan

^CHokkaido University, Laboratory of Nanostructured Functional Materials, Research Institute for Electronic Science (RIES), N20 W10, Kita-ku, Sapporo, Hokkaido 001-0020, Japan

Corresponding authors:

Pedro Baptista de Castro E-mail: CASTRO.Pedro@nims.go.jp
National Institute for Materials Science, 1-2-1 Sengen, Tsukuba, Ibaraki 305-0047, Japan

Kensei Terashima E-mail: TERASHIMA.Kensei@nims.go.jp
National Institute for Materials Science, 1-2-1 Sengen, Tsukuba, Ibaraki 305-0047, Japan

Effect of Dy substitution in the giant magnetocaloric properties of HoB₂

Recently, a massive magnetocaloric effect near the liquefaction temperature of hydrogen has been reported in the ferromagnetic material HoB₂. Here we investigate the effects of Dy substitution in the magnetocaloric properties of Ho_{1-x}Dy_xB₂ alloys ($x = 0, 0.3, 0.5, 0.7, 1.0$). We find that the Curie temperature (T_C) gradually increases upon Dy substitution, while the magnitude of the magnetic entropy change $|\Delta S_M|$ at $T = T_C$ decreases from 0.35 to 0.15 J cm⁻³ K⁻¹ for a field change of 5 T. Due to the presence of two magnetic transitions in these alloys, despite the change in the peak magnitude of $|\Delta S_M|$, the refrigerant capacity (RC) and refrigerant cooling power (RCP) remains almost constant in all doping range, which as large as 5.5 J cm⁻³ and 7.0 J cm⁻³ for a field change of 5 T. These results imply that this series of alloys could be an exciting candidate for magnetic refrigeration in the temperature range between 10 – 50 K.

Keywords: magnetic refrigeration, magnetocaloric effect

Introduction

Magnetic refrigeration is an emerging environmental friendly technology for refrigeration applications, as it does not require to use greenhouse gases and does not depend on conventional gas compression cycles[1–3] while having possible higher cycle efficiency[1,4]. It is based on the magnetocaloric effect (MCE), which consists of the adiabatic temperature change (ΔT_{ad}) a magnetic material will undergo when a magnetic field is applied/removed adiabatically, but it can also be evaluated in terms of the magnetic entropy change (ΔS_M) this magnetic material will undergo for the same

field change, where ΔS_M usually peaks at the magnetic transition temperature (T_{mag}).

Recently, our group unveiled a giant magnetocaloric effect of $|\Delta S_M^{\text{MAX}}| = 0.35 \text{ J cm}^{-3} \text{ K}^{-1}$ ($40.1 \text{ J kg}^{-1} \text{ K}^{-1}$) in the vicinity of a ferromagnetic transition at the Curie temperature (T_C) of 15 K for a field change of $\mu_0\Delta H = 5 \text{ T}$ in HoB_2 [5]. Due to the closeness of its T_C to the liquefaction point of hydrogen (20.3 K), this material became an attractive candidate for use in low-temperature magnetic refrigeration applications focused on the liquefaction stage of hydrogen. Hydrogen is considered to be one most promising replacement for hydrocarbon fuels as a clean energy source[6,7] and in particular liquid hydrogen is widely needed in the space industry[8] and its liquid form is one the suitable way for transportation and storage[9]. In this context, the discovery of magnetic materials with a high MCE effect at low temperatures is imperative for the development of such refrigerators working at cryogenic temperatures. Since the magnetocaloric effect peaks at T_{mag} , tuning the T_C of HoB_2 to a higher temperature is of extreme interest to examine HoB_2 -based materials as possible candidates for refrigeration before the liquefaction stage, especially below temperatures of 77 K. Since, DyB_2 orders ferromagnetically at $T_C = 50 \text{ K}$ [10,11] and exhibits a $|\Delta S_M|$ of $0.16 \text{ J cm}^{-3} \text{ K}^{-1}$ ($17.1 \text{ J kg}^{-1} \text{ K}^{-1}$) for $\mu_0\Delta H = 5 \text{ T}$ [12], the partial substitution of Ho by Dy is expected to shift T_C to higher values in the expense of a probable reduction of $|\Delta S_M|$. In this work, we study the magnetocaloric properties of $\text{Ho}_{1-x}\text{Dy}_x\text{B}_2$ alloys ($x = 0, 0.3, 0.5, 0.7, 1.0$) and compare with other well-known materials working at the same temperature span.

All the magnetocaloric properties of the samples will be reported in volumetric units ($\text{J cm}^{-3} \text{ K}^{-1}$) as this is the adequate unit when comparing materials for application purposes as there is a volume limit when constructing real applications[13,14].

Therefore, herein all comparisons with other materials will be done in this unit by converting it using the ideal density of each material when not provided.

Experimental Section

Sample Synthesis

Polycrystalline samples of $\text{Ho}_{1-x}\text{Dy}_x\text{B}_2$ were prepared by an arc-melting process in a water-cooled copper hearth arc furnace under Ar atmosphere. Stoichiometric amounts of Ho (99.9% purity), Dy (99.9% purity), and B (99.5% purity) were weighted and then arc melted several times. During the process of sample synthesis, we found out that annealing the samples under different conditions did not change the X-ray diffraction patterns of the obtained samples, therefore no annealing procedure was carried out in the samples in this work.

Characterization

Powder X-ray diffraction (XRD) patterns of the arc melted samples were investigated using a Rigaku-MiniFlex 600 with $\text{Cu K}\alpha$ radiation. The lattice parameters, the volume of the unit cell, and density were obtained by refining the XRD patterns using the FULLPROF[15] software.

Magnetization Measurements

Magnetization measurements were carried out by a superconducting quantum interference device magnetometer contained in the Magnetic Property Measurement System XL (Quantum Design). Zero-field cooling (ZFC) and field cooling (FC) measurement at low fields were taken to evaluate the evolution of T_C as a function of

Dy content. For the evaluation of $|\Delta S_M|$ the magnetization measurements of the sample under various applied fields ranging from 0.01 to 5 T were performed in ZFC process.

Results and Discussion

Crystal Structure

Fig. 1 (a) shows the XRD patterns for the obtained arc melted samples. The main phase peaks can be indexed into a hexagonal $P6/mmm$ $A1B_2$ type crystal structure as shown by the red fitting curves. The remaining peaks are assigned as REB_4 , unreacted RE or RE_2O_3 (RE = Ho, Dy) impurity peaks marked by a black square (■), a black star (★), or a black diamond (◆) respectively. The obtained lattice parameters, the volume of the unit cell, and density are summarized in Table 1.

As shown in Table 1, Dy substitution in the Ho site seems to strongly affect the c -axis length while the a -axis length weakly changes, illustrated in Fig. 1 (b) where we plot the normalized lattice parameters (a/a_0 and c/c_0) by the value of $x = 0$. Both c/c_0 and a/a_0 increases with x , roughly following the so-called Vegard's law (marked by the dashed black line), but with different rates. The observed changes in the lattice constants in $Ho_{1-x}Dy_xB_2$ suggests that the substitution of Ho by Dy in the REB_2 main phase was successful, and these partially substituted samples can be in the form of a random alloy. We note that in the case of $HoB_{2-x}Si_x$ solid solutions[10] where B site is partially substituted, it has been reported that the expansion rate of a -axis length and c -axis length are comparable to each other. This difference in the change of lattice constants between $Ho_{1-x}Dy_xB_2$ and $HoB_{2-x}Si_x$ implies that the a -axis and c -axis lengths in HoB_2 -based compounds might be closely related to the bonds along axes. Namely, c -

axis length seems to be depending on Ho-B bonds and be sensitive to both rare-earth and B-site atoms, while the a -axis length might be more dependent on the B site atom.

Magnetic Properties

The ZFC-FC isofield magnetization (M - T) for an applied field of $\mu_0 H = 0.01$ T and isothermal magnetization (M - H) at $T = 5$ K are shown in Fig. 2 (a-e) and (f-g) for each obtained sample respectively. For the Dy containing samples, the divergence between the ZFC and FC M - T curves becomes more pronounced and a small magnetic hysteresis in the M - H curves is observed, including the end-material DyB₂.

To evaluate the of the magnetic transition temperatures in this system, the temperature-dependent derivative of the ZFC curves were taken and are shown in the lower panels of Fig. 2 (a-e). The Curie temperatures, that are defined by the peak position in $\partial M/\partial T$ curves marked by the T_C arrows, showing a systematic increase with Dy content. On the other hand, a second magnetic transition marked by T^* that is observed at lower temperatures, which is also observed at HoB₂ at $T^* = 11$ K[5] and DyB₂ at $T^* = 15$ K[12], seems to be almost unchanged by partial substitution of Dy. The origin of T^* was attributed to a possible spin-reorientation mechanism[12], however, the nature of this transition is still unknown and its investigation is outside the scope of this work. The Dy doping dependence of both transitions is summarized in Fig. 3 showing the monotonic increase of T_C until 50 K, while T^* remains almost constant.

Magnetocaloric Properties

For evaluating the magnetocaloric effect of the obtained samples, M - T curves in a wide range of applied magnetic fields were measured for all samples, shown in Fig. 4 (a-e) and $|\Delta S_M|$ was calculated using the Maxwell relation:

$$\Delta S_M = \mu_0 \int_0^H \left(\frac{\partial M}{\partial T} \right)_H dH \quad (1).$$

The obtained $|\Delta S_M|$ for fields ranging from 0 to 5 T is shown in Fig. 4 (f-g).

Due to the presence of the two transitions at T^* and T_C , two peaks appear at $|\Delta S_M|$. Therefore, here we will define and compare the maximum entropy change $|\Delta S_M^{MAX}|$ as $|\Delta S_M(T = T_C)|$, since T^* remains almost unchanged during the whole doping range and is always lower than 15 K while we are interested in the $|\Delta S_M|$ peak shifted toward higher temperature by Dy doping. In this way, the obtained values of $|\Delta S_M^{MAX}|$ for $\mu_0\Delta H = 5$ T were 0.35, 0.3, 0.18, 0.16 and 0.15 J cm⁻³ K⁻¹ for $x = 0, 0.3, 0.5, 0.7$ and 1.0 respectively.

In addition to the change in the magnitude of $|\Delta S_M^{MAX}|$, an interesting characteristic appears in the $|\Delta S_M|$ curves of Ho_{1-x}Dy_xB₂. That is, since there are multiple transitions in this series of alloys, even though there is a net loss at $|\Delta S_M^{MAX}|$, the entropy change curve shows an increase of δT_{FWHM} , defined as the region in the entropy curve where $|\Delta S_M| \geq |\Delta S_M^{MAX}|/2$, leading to a gain in maximum entropy change for higher temperature spans. Such a widening of the $|\Delta S_M|$ curves due to multiple transitions has been commonly observed in materials that show more than one magnetic transition [16–18] and it tends to lead to a high figure of merits. The $|\Delta S_M|$ for all samples for a field change of $\mu_0\Delta H = 5$ T is shown in Fig. 5.

Here we consider the two most commonly used figures of merit for evaluating magnetocaloric materials, (i) the refrigerant capacity[1,2,19] (RC) defined as $RC = - \int_{T_{cold}}^{T_{hot}} \Delta S_M dT$, where the usual values of T_{cold} and T_{hot} are the ones defined by δT_{FWHM} (as such, $\delta T_{FWHM} = T_{hot} - T_{cold}$), that tries to represent the amount of heat that can be transferred from the cold sink to the hot sink in an ideal thermodynamic cycle, and (ii) the relative cooling power[1,20–22] (RCP): $RCP (S) = \Delta S_M^{MAX} * \delta T_{FWHM}$. For a field change of $\mu_0\Delta H = 5$ T, the obtained values of RC and RCP on Ho_{1-x}Dy_xB₂ are

summarized in Table 2 where it clearly shows that due to the increase of δT_{FWHM} , they stay almost the same for the whole doping range, indicating that the loss in maximum $|\Delta S_M|$ is compensated by the increase of δT_{FWHM} .

Let us compare the magnetocaloric property values of $|\Delta S_M^{MAX}|$, RC , RCP , and T_{mag} in $Ho_{1-x}Dy_xB_2$ with those of representative materials that are often considered for magnetic refrigeration applications, such as RAI_2 (R=rare-earth) series and materials that exhibit high values of $|\Delta S_M|$ with transition temperatures ranging up to 77 K, based on Fig. S5 of Ref [5]. For this purpose, the values of entropy change are converted into volumetric units by using the density contained in the AtomWork[23] database, unless otherwise provided by the authors. Also, the values of RC/RCP and δT_{FWHM} are estimated from the reported within the contained references when not reported by the authors and they are all summarized in Table 2.

At the temperature range of 15- 20 K, HoB_2 and $Ho_{0.7}Dy_{0.3}B_2$ show a higher figure of merit by a large margin, for $\mu_0\Delta H = 5$ T, when compared to compounds with similar T_{mag} such as $ErAl_2$ [24], $TmGa$ [25], EuS [26], HoN [27] and $DyNi_2$ [24]. For the materials with transition temperatures around 30 K, $Ho_{0.5}Dy_{0.5}B_2$ also shows a significantly larger figure of merit than the compounds with similar T_{mag} such as $HoAl_2$ [28] and $ErCo_2$ [29]. On the other hand, $Ho_{0.3}Dy_{0.7}B_2$ shows similar performance to the intermetallic compound $HoNi$ [30], but both of them surpass the $ErCo_2$ -based alloy $Er_{0.53}Ho_{0.47}Co_2$ [31]. In the case of DyB_2 , even though it shows almost half of $|\Delta S_M|$ compared to Gd_3Ru [32], the figure of merits in those two compounds are comparable to each other, and both vastly outperform those values in the Laves phase compound $DyAl_2$ [33]. Note, that here these compounds were selected for comparison for exhibiting the highest $|\Delta S_M^{MAX}|$ with similar transition temperature to the alloys the Ho-Dy-B alloys, to the best of our knowledge, or for being already used in magnetic

refrigeration prototypes. In most of the mentioned cases, even when the $|\Delta S_M^{\text{MAX}}|$ of the Ho-Dy-B alloys is lower, their figure of merit is, higher by a larger margin. In addition, it should be noted that even among compounds with successive magnetic transitions with similar $|\Delta S_M^{\text{MAX}}|$ such as $\text{Ho}_2\text{Cu}_2\text{Cd}$ [18], ErGa [34] and $\text{Ho}_2\text{Au}_2\text{In}$ [35], $\text{Ho}_{1-x}\text{Dy}_x\text{B}_2$ show remarkably high RC/RCP values. (See Table 2).

Thus, these results indicate that $\text{Ho}_{1-x}\text{Dy}_x\text{B}_2$ alloys have a great potential for use in magnetic refrigeration ranging from 10 to 55 K when compared to the similar materials with T_{mag} within this range, making these compounds as useful as other compounds with giant $|\Delta S_M|$ values in this temperature range such as ErCo_2 and Gd_3Ru .

Conclusions

In this work, we evaluate systematically the effects of Dy substitution on the giant magnetocaloric effect of HoB_2 . Even if there is a net loss in the peak value of the $|\Delta S_M|$, due to the increase of δT_{FWHM} in these alloys, the RC and RCP remain extremely high compared to compounds working in a similar temperature range. Therefore, this series of alloys would have a high potential to work as magnetic refrigerants in the temperature range from 10-50 K.

Acknowledgments

We acknowledge fruitful discussions with Mohammed Elmassalami. This work was partly supported by the JST-Mirai Program “Development of advanced hydrogen liquefaction system by using magnetic refrigeration technology”, the JSPS KAKENHI, and the JST-CREST. P.B. Castro acknowledges the scholarship support from the Ministry of Education, Culture, Sports, Science and Technology (MEXT), Japan.

Disclosure Statement

The authors declare no conflict of interest

Funding

This work was supported by the JST-Mirai Program (Grant No. JPMJMI18A3), JSPS KAKENHI (Grant Nos. 19H02177, 20K05070), JST CREST (Grant No. JPMJCR20Q4)

References

- [1] Gschneidner KA, Pecharsky VK. Magnetocaloric Materials. *Annu. Rev. Mater. Sci.* 2000;30:387–429.
- [2] Franco V, Blázquez JS, Ipus JJ, et al. Magnetocaloric effect: From materials research to refrigeration devices. *Prog. Mater. Sci.* 2018;93:112–232.
- [3] Tegos O, Brück E, Buschow KHJ, et al. Transition-metal-based magnetic refrigerants for room-temperature applications. *Nature.* 2002;415:150–152.
- [4] Numazawa T, Kamiya K, Utaki T, et al. Magnetic refrigerator for hydrogen liquefaction. *Cryogenics (Guildf).* 2014;62:185–192.
- [5] Castro PB de, Terashima K, Yamamoto TD, et al. Machine-learning-guided discovery of the gigantic magnetocaloric effect in HoB₂ near the hydrogen liquefaction temperature. *NPG Asia Mater.* 2020;12:35.
- [6] Johnston B, Mayo MC, Khare A. Hydrogen: the energy source for the 21st century. *Technovation.* 2005;25:569–585.
- [7] Jones LW. Liquid hydrogen as a fuel for the future. *Science (80-.).*

1971;174:367–370.

- [8] Shirron PJ. Applications of the magnetocaloric effect in single-stage, multi-stage and continuous adiabatic demagnetization refrigerators. *Cryogenics (Guildf)*. 2014;62:130–139.
- [9] Sherif SA, Zeytinoglu N, Veziroğlu TN. Liquid hydrogen: Potential, problems, and a proposed research program. *Int. J. Hydrogen Energy*. 1997;22:683–688.
- [10] Roger J, Babizhetskyy V, Guizouarn T, et al. The ternary RE-Si-B systems (RE = Dy, Ho, Er and Y) at 1270 K: Solid state phase equilibria and magnetic properties of the solid solution $REB_{2-x}Si_x$ (RE = Dy and Ho). *J. Alloys Compd*. 2006;417:72–84.
- [11] Novikov V V., Matovnikov A V., Volkova OS, et al. Synthesis, thermal and magnetic properties of RE-diborides. *J. Magn. Magn. Mater*. 2017;428:239–245.
- [12] Meng H, Li B, Han Z, et al. Reversible magnetocaloric effect and refrigeration capacity enhanced by two successive magnetic transitions in DyB_2 . *Sci. China Technol. Sci*. 2012;55:501–504.
- [13] Gschneidner A, Pecharsky VK, Tsokol AO. Recent developments in magnetocaloric materials. *Reports Prog. Phys*. 2005;68:1479–1539.
- [14] Gottschall T, Skokov KP, Fries M, et al. Making a Cool Choice: The Materials Library of Magnetic Refrigeration. *Adv. Energy Mater*. 2019;9:1901322.
- [15] Carvajal J. FULLPROF: A Program for Rietveld Refinement and Pattern Matching Analysis. *Abstr. Satell. Meet. Powder Diffr. XV Congr. IUCr*. 1990. p. 127.

- [16] Zheng XQ, Chen J, Shen J, et al. Large refrigerant capacity of RGa ($R = Tb$ and Dy) compounds. *J. Appl. Phys.* 2012;111:07A917.
- [17] Zhang Y, Xu X, Yang Y, et al. Study of the magnetic phase transitions and magnetocaloric effect in Dy_2Cu_2In compound. *J. Alloys Compd.* 2016;667:130–133.
- [18] Yi Y, Li L, Su K, et al. Large magnetocaloric effect in a wide temperature range induced by two successive magnetic phase transitions in Ho_2Cu_2Cd compound. *Intermetallics.* 2017;80:22–25.
- [19] Pecharsky VK, Gschneidner KA. Some common misconceptions concerning magnetic refrigerant materials. *J. Appl. Phys.* 2001;90:4614–4622.
- [20] Phan M-H, Yu S-C. Review of the magnetocaloric effect in manganite materials. *J. Magn. Magn. Mater.* 2007;308:325–340.
- [21] Niknia I, Trevizoli P V., Christiaanse T V., et al. Material screening metrics and optimal performance of an active magnetic regenerator. *J. Appl. Phys.* 2017;121:064902.
- [22] Monfared B, Palm B. Material requirements for magnetic refrigeration applications. *Int. J. Refrig.* 2018;96:25–37.
- [23] Xu Y, Yamazaki M, Villars P. Inorganic Materials Database for Exploring the Nature of Material. *Jpn. J. Appl. Phys.* 2011;50:11RH02.
- [24] von Ranke PJ, Pecharsky VK, Gschneidner KA. Influence of the crystalline electrical field on the magnetocaloric effect of $DyAl_2$, $ErAl_2$ and $DyNi_2$. *Phys. Rev. B.* 1998;58:12110–12116.

- [25] Mo Z-J, Shen J, Yan L-Q, et al. Low field induced giant magnetocaloric effect in TmGa compound. *Appl. Phys. Lett.* 2013;103:52409.
- [26] Li DX, Yamamura T, Nimori S, et al. Large reversible magnetocaloric effect in ferromagnetic semiconductor EuS. *Solid State Commun.* 2014;193:6–10.
- [27] Yamamoto TA, Nakagawa T, Sako K, et al. Magnetocaloric effect of rare earth mono-nitrides, TbN and HoN. *J. Alloys Compd.* 2004;376:17–22.
- [28] Gil LA, Campoy JCP, Plaza EJR, et al. Conventional and anisotropic magnetic entropy change in HoAl₂ ferromagnetic compound. *J. Magn. Magn. Mater.* 2016;409:45–49.
- [29] Wada H, Tanabe Y, Shiga M, et al. Magnetocaloric effects of Laves phase Er(Co_{1-x}Ni_x)₂ compounds. *J. Alloys Compd.* 2001;316:245–249.
- [30] Rajivgandhi R, Arout Chelvane J, Quezado S, et al. Effect of rapid quenching on the magnetism and magnetocaloric effect of equiatomic rare earth intermetallic compounds RNi (R = Gd, Tb and Ho). *J. Magn. Magn. Mater.* 2017;433:169–177.
- [31] Matsumoto K, Numazawa T. Magnetic Refrigerator for Hydrogen Liquefaction. *TEION KOGAKU (Journal Cryog. Supercond. Soc. Japan)*. 2015;50:66–71.
- [32] Monteiro JCB, dos Reis RD, Gandra FG. The physical properties of Gd₃Ru: A real candidate for a practical cryogenic refrigerator. *Appl. Phys. Lett.* 2015;106:194106.
- [33] Hashimoto T, Matsumoto K, Kurihara T, et al. Investigations on the Possibility of the RAl₂ System as a Refrigerant in an Ericsson Type Magnetic Refrigerator.

- [34] Chen J, Shen BG, Dong QY, et al. Large reversible magnetocaloric effect caused by two successive magnetic transitions in ErGa compound. Appl. Phys. Lett. 2009;95:132504.
- [35] Li L, Yi Y, Su K, et al. Magnetic properties and large magnetocaloric effect in Ho₂Cu₂In and Ho₂Au₂In compounds. J. Mater. Sci. 2016;51:5421–5426.

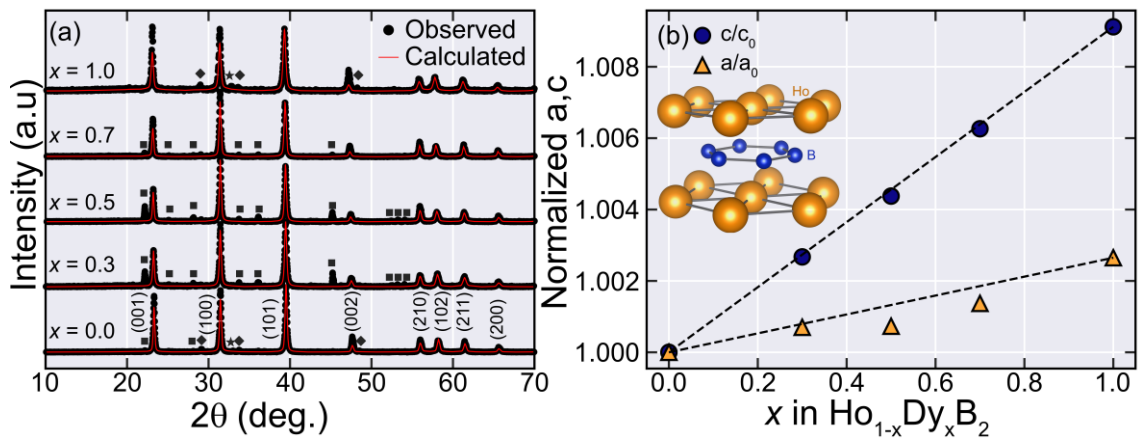


Figure 1. Powder XRD patterns and lattice constant evolution for Ho_{1-x}Dy_xB₂ alloys.

(a) XRD patterns of the obtained alloys. The red lines show the calculated patterns from Rietveld refinement for the REB₂ main phase. The black square (■) marks an REB₄ impurity phase, while the black star (★) marks a RE impurity peak and the black diamond (◆) marks a RE₂O₃ impurity peak (RE=Ho, Dy). (b) The lattice parameters normalized by the value at $x = 0$, as a function of x . The black dashed line shows a guide based on Vegard's law, given by $1 - x + x \left(\frac{a_1, c_1}{a_0, c_0} \right)$ where $(a, c)_{0,1}$ is the lattice constants at $x = 0$ or 1.

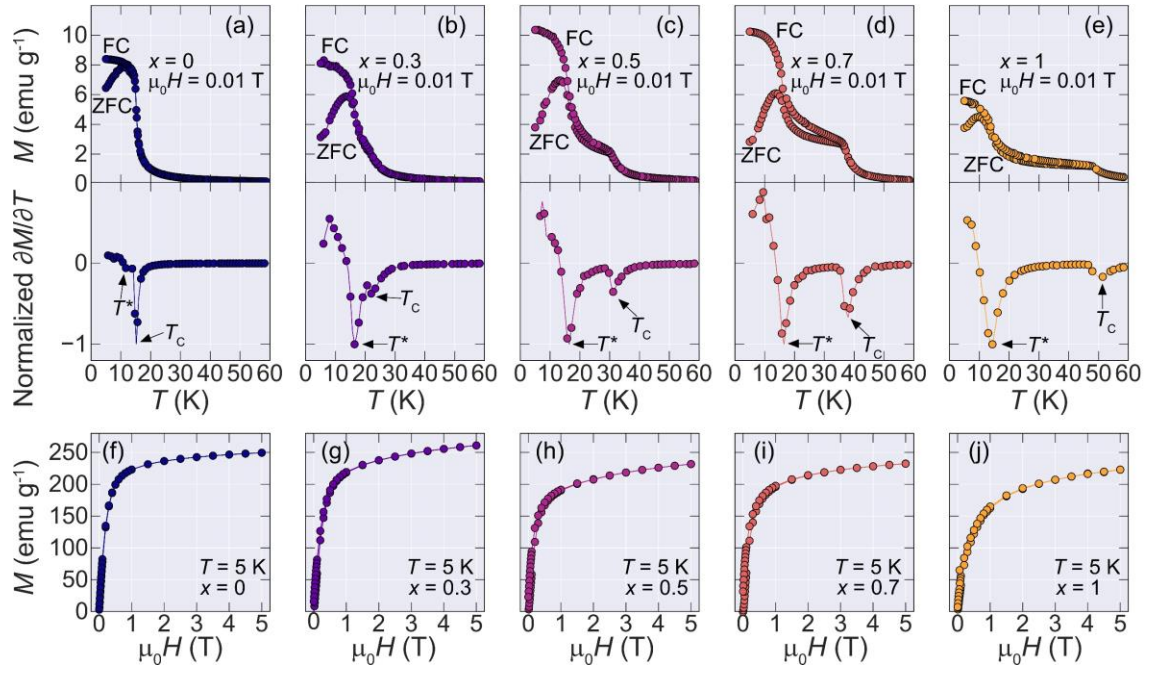


Figure 2. Isofield (M - T) ZFC-FC, Normalized temperature-dependent derivatives of the ZFC curves, and Isothermal (M - H) magnetization curves of $\text{Ho}_{1-x}\text{Dy}_x\text{B}_2$ alloys. (a-e) ZFC and FC curves for all synthesized alloys for an applied field of $\mu_0 H = 0.01$ T. The lower panels show the derivatives of the ZFC curves normalized by the minimum of the derivative value. The two magnetic transitions T_C and T^* , are marked by the arrows. (f-g) Isothermal magnetization at $T = 5$ K.

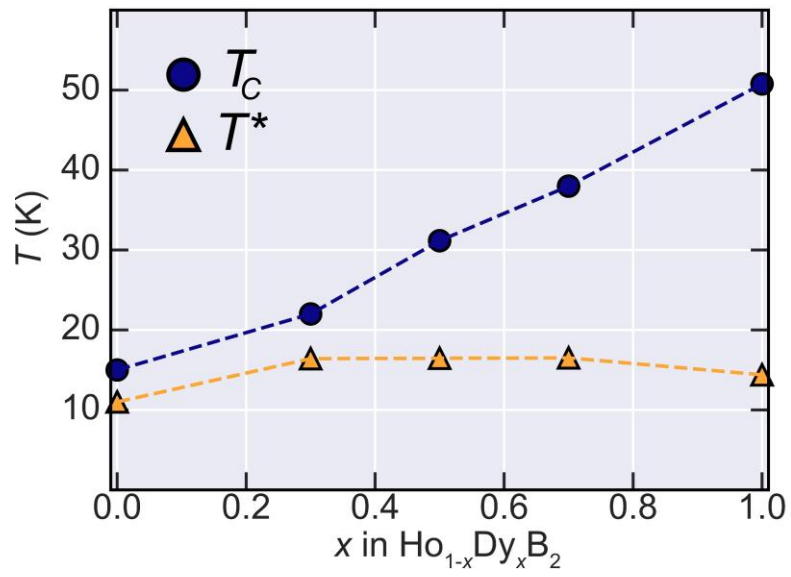


Figure 3. Phase diagram between ordering temperature and doping amount (x) for $\text{Ho}_{1-x}\text{Dy}_x\text{B}_2$. The blue filled circles show the evolution of T_C while the yellow triangles show T^* . While T_C increases monotonically with x , T^* remains almost constant.

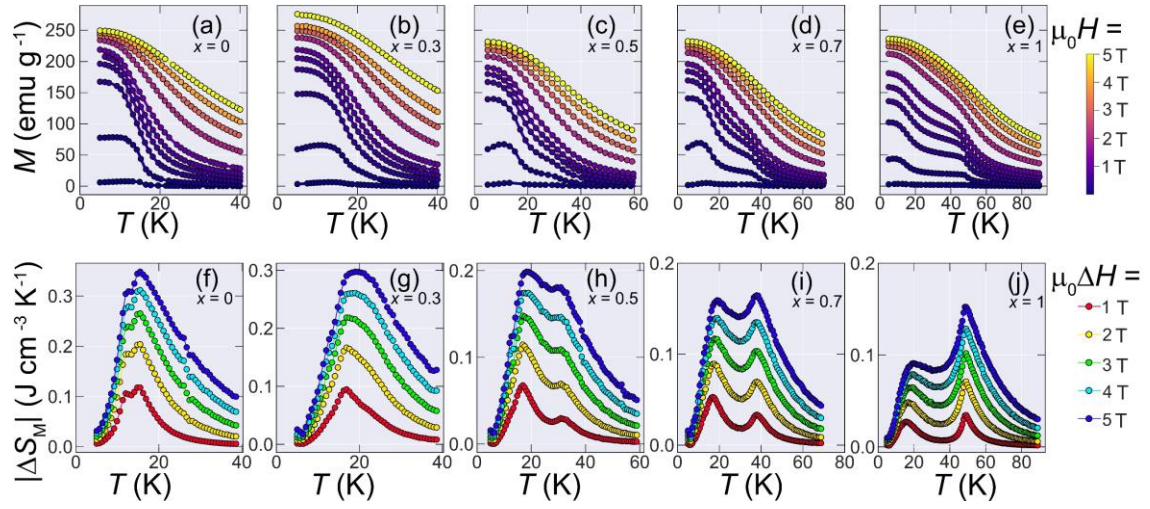


Figure 4. M - T curves at a vast range of applied fields and obtained magnetic entropy change for $\text{Ho}_{1-x}\text{Dy}_x\text{B}_2$ alloys. (a-e) The obtained M - T curves measured by ZFC process from $\mu_0 H = 5$ T to 0.01 T. (f-j) Magnetic entropy changes for $\text{Ho}_{1-x}\text{Dy}_x\text{B}_2$ alloys for $\mu_0 \Delta H$ ranging from 1 to 5 T obtained from the M - T curves of (a-e). With the increase of Dy content, the maximum value of $|\Delta S_M|$ decreases from $0.35 \text{ J cm}^{-3} \text{ K}^{-1}$ ($x = 0$) to $0.16 \text{ J cm}^{-3} \text{ K}^{-1}$ ($x = 1.0$).

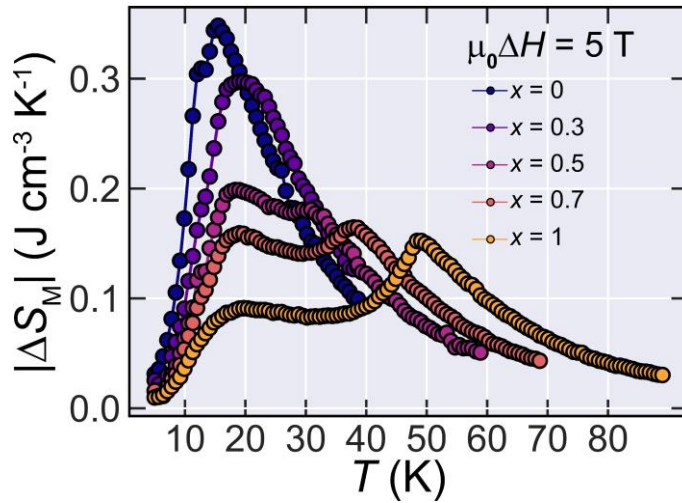


Figure 5. $|\Delta S_M|$ at $\mu_0 \Delta H = 5$ T for $\text{Ho}_{1-x}\text{Dy}_x\text{B}_2$ alloys.

Nominal Dy (x)	a (Å)	c (Å)	V (Å ³)	ρ (g/cm ³)
0	3.283(3)	3.815(8)	35.62(4)	8.696
0.3	3.285(6)	3.827(1)	35.77(8)	8.626
0.5	3.285(7)	3.832(5)	35.82(9)	8.591
0.7	3.287(8)	3.839(7)	35.94(7)	8.540
1.0	3.292(0)	3.850(6)	36.14(0)	8.461

Table 1: Obtained lattice parameters from XRD patterns for Ho_{1-x}Dy_xB₂

Material	T_{mag} (K)	$\Delta S_M^{\text{MAX}} $ (J cm ⁻³ K ⁻¹)	δT_{FWHM} (K)	RC (J cm ⁻³)	RCP (J cm ⁻³)	Ref
HoB ₂	15	0.35	18.9	5.1	6.6	This work
Ho _{0.7} Dy _{0.3} B ₂	22	0.30	23.5	5.5	7.0	This work
Ho _{0.5} Dy _{0.5} B ₂	31	0.18	32.8	5.5	6.3	This work
Ho _{0.3} Dy _{0.7} B ₂	37	0.16	42.7	5.8	7.0	This work
DyB ₂	50	0.15	51.2	5.1	7.8	This work
ErAl ₂	14	0.22 ^a	15.4 ^b	2.7 ^{a,b}	3.5 ^{a,b}	24
TmGa	15	0.3 ^a	14.6 ^b	3.2 ^a	4.4 ^{a,b}	25
EuS	18	0.21 ^a	20.9 ^b	3.4 ^b	4.5 ^a	26
HoN	18	0.29	19.9	4.4 ^b	5.7 ^b	27

DyNi ₂	21 ^b	0.24 ^{a,b}	21.4 ^b	3.8 ^{a,b}	5.0 ^{a,b}	24
Ho ₂ Au ₂ In	21	0.16 ^a	26.7	3.0 ^a	4.2 ^a	35
Ho ₂ Cu ₂ Cd	30	0.18 ^a	23.6 ^b	3.0 ^a	4.3 ^a	18
ErGa	30	0.18 ^a	0.18 ^a	4.2 ^a	5.6 ^{a,b}	34
HoAl ₂	30	0.15 ^{a,b}	31.8 ^{b-}	3.6 ^{a,b}	4.9 ^{a,b}	28
ErCo ₂	30	0.37 ^{a,b}	10.1 ^b	3.2 ^{a,b}	3.8 ^{a,b}	29
HoNi	36	0.17 ^a	42.3 ^b	5.2 ^{a,b}	7.3 ^{a,b}	30
Er _{0.53} Ho _{0.47} Co ₂	35 ^d	0.22 ^b	15.1 ^b	3.0 ^b	3.5 ^b	31
Gd ₃ Ru	54	0.26	23.5 ^b	5.2 ^b	6.1	32
DyAl ₂	56	0.11 ^{a,b}	42.3 ^b	3.8 ^{a,b}	4.9 ^{a,b}	33

Table 2: Values of $|\Delta S_M^{\text{MAX}}|$, δT_{FWHM} , RC and RCP for Ho_{1-x}Dy_xB₂ and representative compounds with similar transitions temperatures. All the data is expressed in volumetric units. a: Converted to volumetric units using ideal density contained in the AtomWork database. b: Estimated from the $|\Delta S_M|$ curves reported in the reference.